



Impacts of fire emissions and transport pathways on the interannual variation of CO in the tropical upper troposphere

L. Huang^{1,2}, R. Fu¹, and J. H. Jiang²

¹Jackson School of Geosciences, The University of Texas at Austin, Austin, TX, USA

²Jet Propulsion Laboratory, California Institute of Technology, Pasadena, CA, USA

Correspondence to: L. Huang (leih@utexas.edu)

Received: 30 August 2013 – Published in Atmos. Chem. Phys. Discuss.: 7 October 2013

Revised: 8 March 2014 – Accepted: 10 March 2014 – Published: 25 April 2014

Abstract. This study investigates the impacts of fire emission, convection, various climate conditions and transport pathways on the interannual variation of carbon monoxide (CO) in the tropical upper troposphere (UT), by evaluating the field correlation between these fields using multi-satellite observations and principle component analysis, and the transport pathway auto-identification method developed in our previous study. The rotated empirical orthogonal function (REOF) and singular value decomposition (SVD) methods are used to identify the dominant modes of CO interannual variation in the tropical UT and to study the coupled relationship between UT CO and its governing factors. Both REOF and SVD results confirm that Indonesia is the most significant land region that affects the interannual variation of CO in the tropical UT, and El Niño–Southern Oscillation (ENSO) is the dominant climate condition that affects the relationships between surface CO emission, convection and UT CO. In addition, our results also show that the impact of El Niño on the anomalous CO pattern in the tropical UT varies strongly, primarily due to different anomalous emission and convection patterns associated with different El Niño events. In contrast, the anomalous CO pattern in the tropical UT during La Niña period appears to be less variable among different events. Transport pathway analysis suggests that the average CO transported by the “local convection” pathway ($\Delta\text{CO}_{\text{local}}$) accounts for the differences of UT CO between different ENSO phases over the tropical continents during biomass burning season. $\Delta\text{CO}_{\text{local}}$ is generally higher over Indonesia–Australia and lower over South America during El Niño years than during La Niña years. The other pathway (“advection within the lower troposphere followed by convective vertical transport”) occurs more frequently over

the west-central Pacific during El Niño years than during La Niña years, which may account for the UT CO differences over this region between different ENSO phases.

1 Introduction

Carbon monoxide (CO), which is a byproduct of the incomplete combustion of carbon-based fuels, plays an important role in atmospheric chemistry and radiation balance. CO is one of the ozone (O_3) precursors (Daniel and Solomon, 1998) and is also the primary sink of the hydroxyl radical (OH) (Thompson, 1992). With a lifetime of 1–2 months in the troposphere, CO is an excellent tracer to study the mass transport of polluted air originating in regions of biomass burning or fossil fuel combustion (Edwards et al., 2006a). Thus, understanding the factors that control CO temporal and spatial variations is important for improving numerical model simulations and predictions of tropospheric ozone change and fire-generated pollutant transport.

Besides strong seasonal variations as shown by previous studies (Novelli et al., 1998; Schoeberl et al., 2006; Liu et al., 2007, 2010; Huang et al., 2012), CO has also been shown to have large interannual variability in the troposphere (Wotawa et al., 2001; Edwards et al., 2006b; Duncan and Logan, 2008; Liu et al., 2013). Edwards et al. (2006b) found that the interannual variation of tropospheric CO in the Southern Hemisphere (SH) has a significant correlation with the El Niño–Southern Oscillation (ENSO) precipitation index. Duncan and Logan (2008) analyzed the factors that regulate the trends and interannual variability of tropospheric CO for 1988–1997 through a model study, and found the

interannual variation of biomass burning, especially those major burning events in Indonesia associated with El Niño, is the main driver of large-scale CO variability in the tropics. Strong interannual variation of CO in the upper troposphere (UT) is found to be mainly related to the intense drought-induced fires in Indonesia and South America (Liu et al., 2013; Livesey et al., 2013).

Recent studies (e.g., Ashok et al., 2007; Kao and Yu, 2009; Kug et al., 2009) have shown that the canonical El Niño (eastern Pacific warming) has become less frequent, and a different kind of El Niño (central Pacific warming) has become more common during the late 20th century. These two types of El Niño have distinctively different anomalous large-scale circulation and convection patterns (Yeh et al., 2009; Su and Jiang, 2013), which would in turn have different impacts on CO transport to the UT. What are the differences between the impacts of different ENSO phases on the interannual variation of tropical UT CO? The answer to this question may help to reconcile the discrepancies in previous studies about how ENSO would affect CO in the UT. For example, Chandra et al. (2009) attributed the change of UT CO to increased fires and meteorological changes over the Indonesian region during the 2006 El Niño, while Duncan et al. (2007) suggested that an increase of convective transport of CO emitted over South America and Africa due to an eastward shift of convective center in the Pacific closer to these fires source regions also played an important role in the increase of UT CO during the 1997 El Niño.

Although fires in tropical Africa and South America have important influences on the seasonal peaks of UT CO, how they would affect the interannual variation of UT CO has not been thoroughly investigated. Gonzi and Palmer (2010) suggested that the fractions of surface CO emissions transported to the UT are lower over Africa and South America than over tropical Asia. However, Ricaud et al. (2007) found that deep convection plays an important role in transporting CO to the UT over Africa, which suggests a change of emission and convection over this region could significantly influence UT CO. Thus, how changes of fire emissions over these two tropical continents contribute to the changes of CO in the UT needs to be clarified.

Interannual variations of atmospheric circulation can also influence CO transport pathways (e.g., Duncan et al., 2007; Liu et al., 2013). The relative importance between changes of surface emission and transport pathways on the interannual changes of UT CO and how such relative importance varies with, for example, different ENSO phases, is still an open question. Previous studies have shown that CO is transported from the surface to the UT through two pathways: the “local convection” pathway (Thompson et al., 1996; Pickering et al., 1996; Andreae et al., 2004) and the “lower troposphere (LT) advection → convection” pathway (Folkins et al., 1997; Andreae et al., 2001). The former refers to CO being transported from the surface to the UT by local deep convection over fire regions, whereas the latter refers to CO being ad-

ducted from a fire region to a convective region within the LT, and then being uplifted to the UT by deep convection. This “LT advection → convection” pathway may be responsible for the fact that UT CO centers are often located above convective regions rather than fire regions. Huang et al. (2012) developed a method to automate the identification of these pathways through a joint use of A-Train multi-satellite measurements. This approach allows us to more efficiently evaluate the relationships between changes of CO emission, transport pathways and CO in the UT.

Most of the previous studies discussed above have a strong focus on ENSO effects. This study explores an objective principle-component-analysis-based approach to identify the dominant modes of the CO interannual variation in the tropical UT and their links to modes of interannual climate variability, such as ENSO and tropical Atlantic variability. In addition, the impacts of different ENSO phases on CO transport to the UT are also evaluated. Section 2 of this paper introduces the data and methods used in this study. Section 3 identifies the dominant modes of the interannual variation of UT CO and evaluates the relative importance of CO emission, convection and continental regions that affect UT CO interannual variation over the tropics. The impacts of CO emission, convection and sea surface temperature (SST) on UT CO interannual variation are analyzed in Sect. 4. The circulation pattern changes and the transport pathway differences associated with different ENSO phases are investigated and discussed in Sect. 5. The main conclusions of this work are summarized and discussed in Sect. 6.

2 Data and methodology

2.1 Data

We use CO volume mixing ratio measurements from Aura Microwave Limb Sounder (MLS) to determine the concentration of CO in the UT, use MLS cloud ice water content (IWC) and CloudSat cloud water content (CWC) data to determine the strength of deep convection, and use CO emission data from the Global Fire Emission Database (GFED) to determine biomass-burning-emitted CO at the surface.

The MLS instrument is a small radio telescope aboard the Aura satellite, which was launched on 15 July 2004, and has a sun-synchronous orbit at an altitude of 705 km, with an Equator crossing time at 1:45 a.m. and 1:45 p.m. local solar time and a 16-day repeat cycle. MLS observes many atmospheric components in the upper troposphere and lower stratosphere (UTLS) by measuring thermal emissions from broad spectral bands with a limb-viewing geometry (Waters et al., 2006). MLS measurement has a vertical resolution of ~4 km for IWC and ~5 km for CO in the UTLS, and a horizontal resolution of ~7 km across-track and 300–400 km along-track. We use level-2 CO and IWC data derived according to the MLS version 3.3 (V3.3) retrieval algorithm

and screen the data using procedures as recommended in Livesey et al. (2011). These include the use of MLS IWC as a filter to exclude cloud-contaminated profiles in CO data screening. The lowest usable retrieval level for CO and IWC is 215 hPa, where the estimated single-measurement precisions are ~ 20 ppbv for CO and $\sim 1 \text{ mg m}^{-3}$ for IWC. The earlier version of MLS CO (V2.2) was biased high by a factor of ~ 2 at 215 hPa (Livesey et al., 2008), but this bias has been largely eliminated in V3.3 CO data (Livesey et al., 2011). Only thick clouds that are typically associated with deep convective cores are observable by MLS (Wu et al., 2008); thus MLS IWC is used as a proxy of deep convection in this study.

CloudSat was launched on 28 April 2006, which carries the first space-borne 94 GHz cloud profiling radar to measure vertical profiles of cloud and precipitation properties, with a vertical resolution of 500 m (Stephens et al., 2002). The CloudSat measurements are reported on an increment of 240 m, with a total of 125 vertical layers. The footprint of a single profile is approximately 1.7 km along-track by 1.3 km across-track, with an along-track sampling every 1.1 km (CloudSat Project, 2008). In this study, CloudSat CWC is calculated as the sum of cloud ice water content and liquid water content observed by CloudSat, and is used to estimate the strength of convective activity in the transport pathway analysis.

The emission of CO by fire activity at the surface is obtained from the Global Fire Emission Database version 3 (GFED3) (van der Werf et al., 2010), currently available from 1997 to 2011. The gridded data have $0.5^\circ \times 0.5^\circ$ spatial resolution and monthly temporal resolution, and include both burned area and fire emissions. Emissions of fire-generated trace gases are derived by combining satellite information on burned area (Giglio et al., 2006, 2010), biogeochemical model estimates of fuel burned, and emission factors for each species. Burned area was derived primarily from the Moderate Resolution Imaging Spectroradiometer (MODIS) on Terra and Aqua satellites (Giglio et al., 2006). In the transport pathway auto-identification method (Huang et al., 2012), daily along-track co-located satellite observations and CO emissions are used. Thus, we need to derive daily emission of CO from GFED3 monthly emission, and the approach we used is described in Mu et al. (2011).

Besides satellite observation data above, we also use monthly mean precipitation and SST data. The precipitation data are from the Global Precipitation Climatology Project (GPCP) (Adler et al., 2003), which are available from 1979 to 2011 and have a horizontal resolution of $2.5^\circ \times 2.5^\circ$. The SST data are obtained from the Optimum Interpolation (OI) SST version 2 (V2) analysis produced by the National Oceanic and Atmospheric Administration (NOAA) using both in situ and satellite data (Reynolds et al., 2002), available from 1981 to present. The spatial resolution of SST data is $1^\circ \times 1^\circ$. In this paper, monthly anomalies of each variable are defined as the deviations from the corresponding climatological monthly mean. The climate indices used in

this paper are obtained from <http://www.esrl.noaa.gov/psd/data/climateindices/list/> and http://www.jamstec.go.jp/frcg/research/d1/iod/DATA/dmi_HadISST.txt.

To homogenize the horizontal resolutions of the MLS CO, IWC, SST and GFED CO emission, we averaged these data into 4° latitude \times 8° longitude grid boxes. The MLS CO and IWC data were also averaged over each month to get the monthly mean.

2.2 Methodology

Empirical orthogonal function (EOF) analysis has been widely used to extract individual modes of variability from data with complex spatial/temporal structures since the first introduction by Lorenz (1956). Rotated EOF (REOF) is a technique simply based on rotating EOFs. It has been adopted by atmospheric scientists since the mid-1980s (Richman, 1986) as an attempt to overcome some of the EOF shortcomings (e.g., domain dependence, difficulty of physical interpretability). Despite the advantages of rotated EOFs, it should be noted that an orthogonal rotation will find a new orthogonal basis, but the principal components (PCs) may not be uncorrelated in the new basis (i.e., the temporal variations associated with each REOF mode are not necessarily independent of the rest). In this study, the REOF analysis was performed using the most well-known and widely used rotation algorithm *varimax* (Kaiser, 1958), which is an orthogonal method, and the first 10 EOFs were chosen for rotation. To identify the dominant modes of the interannual variation of CO in the tropical UT (30°S – 30°N), we apply the REOF analysis to the monthly anomalies of CO at 147 hPa, for the period of August 2004 to July 2012. Singular value decomposition (SVD; Wallace et al., 1992) analysis is usually applied to two combined data fields and identifies pairs of coupled spatial patterns, with each pair explaining a fraction of the total squared covariance between the two fields, which are typically referred to as the left and right field. Projecting the principle component of the left/right field to the original data of its own field yields the homogeneous correlation map, whereas projecting the principle component of the left/right field to the original data of the other field yields the heterogeneous map that describes the coupled relationship between the two fields. The heterogeneous correlation map for the left (right) field represents the correlation between the left (right) field and the principle component of the right (left) field. In this study, we apply the SVD analysis to CO at 147 hPa and different factors (i.e., emission, convection and SST), to investigate the coupled relationship between UT CO and its governing factors. In this way, we can evaluate how interannual variations of CO emission, convection and SST influence the interannual variation of CO in the tropical UT.

The impacts of different climate conditions on the leading REOF and SVD modes of CO in the tropical UT are evaluated using correlation analysis. Although simple linear correlation analysis cannot fully quantify functional relationships,

they could provide an initiative estimation of the relative importance of each variable through the magnitude of correlation coefficient. Since some climate indices (e.g., various ENSO indices) are known to have strong autocorrelation, it is important to estimate the influence of autocorrelation on the significance of the correlation coefficients. To address the autocorrelation issue, we use the methods of both Livezey and Chen (1983, Eqs. 1 and 2) and Bretherton et al. (1999, Eq. 30) to calculate the effective degrees of freedom (EDF) for two time series, and the results are the same for both methods.

The pathway auto-identification method developed in Huang et al. (2012) is used in this study to characterize the differences of CO transport between El Niño and La Niña years. This method identifies the “local convection” pathway when an increase of CO in the UT is detected simultaneously with co-located non-zero surface CO emission and deep convection, and identifies the “LT advection → convection” pathway when an increase of CO in the UT is detected simultaneously only with co-located deep convection (i.e., the co-located surface CO emission is zero). This method streamlines the identification of two CO transport pathways by combining instantaneous along-track observations of CO in the UT from the Aura MLS, convective clouds from the CloudSat radar, and CO emissions derived from the MODIS fire counts data. Thus, it is very useful and efficient for the study of CO transport from the surface to the UT. Further details about this method and its application can be found in Huang et al. (2012).

3 Regions affecting UT CO interannual variation

Figure 1 shows the results of REOF analysis for the monthly anomalies of tropical UT CO at 147 hPa from August 2004 to July 2012. The REOF analysis is applied to the monthly anomalies directly. The first 10 EOF eigenvalues along with their uncertainties are shown in Fig. 1a. We calculated the uncertainty of each eigenvalue based on a rule of thumb (North et al., 1982):

$$\Delta\lambda_k \approx \sqrt{\frac{2}{n}} \lambda_k, \quad (1)$$

where λ_k is the k th eigenvalue, and n is the number of independent samples. Only the first three eigenvalues are well separated from the rest; together they account for 64.5 % of the total monthly UT CO variance. Individually, they explain 37.6 %, 18.6 % and 8.3 % of the total variance (before rotation). After rotation, the three leading REOF modes explain 28.4 %, 13.9 % and 12 % (totally 54.3 %) of the total variance, respectively. Thus, the order of variances explained by the three leading modes did not change; only the magnitudes have a little change. Either way, the three leading modes together explain > 50 % of the total variance. The spatial patterns associated with the first three REOF modes are shown

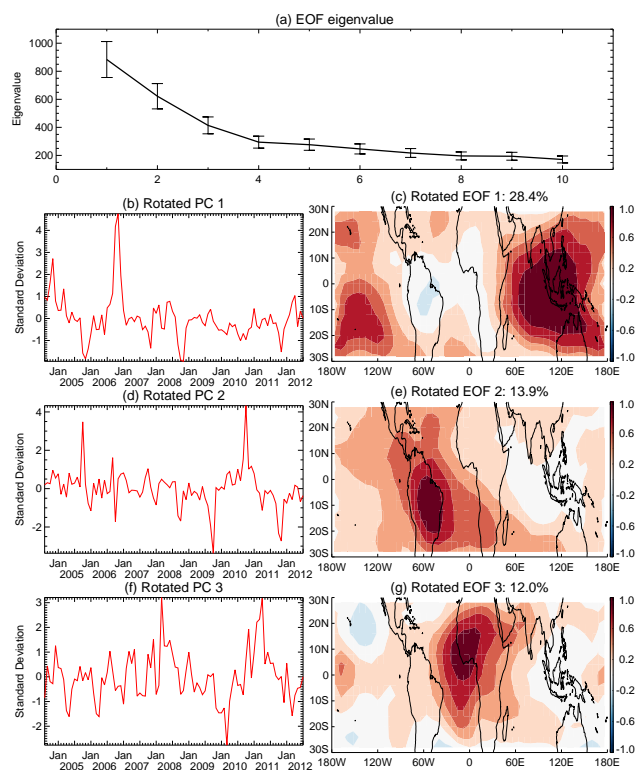


Fig. 1. REOF analysis results of monthly anomalies of CO at 147 hPa for the period of August 2004–July 2012: (a) the first 10 EOF eigenvalues, (b) the first rotated principle component, (c) spatial pattern of the first REOF mode, (d) the second rotated principle component, (e) spatial pattern of the second REOF mode, (f) the third rotated principle component, and (g) spatial pattern of the third REOF mode. The error bars in (a) represent the uncertainties of each eigenvalue. The spatial patterns in (c), (e) and (g) are shown as homogeneous correlation maps.

as homogeneous correlation maps E1, E2 and E3 (Fig. 1c, e, and g), while the temporal variations of each eigenvector are represented by the rotated principal components PC1, PC2 and PC3 (Fig. 1b, d and f). E1 shows two high-correlation centers located over the tropical Indian Ocean, Indonesia and the South Pacific. Since the square of the correlation represents the variance explained locally, this mode accounts for up to 96 % of the variance in the regions of largest amplitude. This is an expected result, since one advantage of REOFs is that they could yield localized or simple structures, and thus highlight the important regions. PC1 is significantly correlated (at 90 % confidence level, the significant correlation is defined at this level hereinafter) with the ENSO indices, after considering the EDF associated with autocorrelation (hereinafter, autocorrelation is considered when needed). For example, the correlation coefficient is -0.36 with Niño 4 Index (EDF = 25, P value = 0.07) and 0.32 with Southern Oscillation Index (SOI) (EDF = 28, P value = 0.08). One possible reason for the relatively weak correlation is that the

dynamic processes that govern CO concentrations in the UT change on an interannual timescale, which leads to complex relationships between tropospheric climate variations and UT CO that are not well captured by simple correlation analysis. The two positive peaks of PC1 indicate the strong impacts of two El Niño events (2004/05 and 2006/07). E2 shows a high-correlation center located over South America (Fig. 1e), which explains up to 86 % of the variance over this region. The two positive peaks of PC2 highlight the impacts of two La Niña events (2005/06 and 2010/11). E3 shows a high-correlation center over West Africa and tropical Atlantic Ocean, explaining up to 86 % of the variance (Fig. 1g). The three peaks of PC3 capture one El Niño event and two La Niña events (2007/08, 2009/10 and 2010/11). Overall, this REOF analysis suggests that the interannual variation of tropical UT CO is significantly affected by changes over the three tropical land regions and various climate conditions such as ENSO. The changes of UT CO over tropical Asia have the largest contribution, whereas those over South America and Africa have a secondary yet significant contribution.

To evaluate the relative importance of emission and convection on the UT CO interannual variation, we analyzed the time series of monthly anomalies of GFED CO emissions, MLS CO at 147 hPa and IWC at 215 hPa over South America (15° S–12° N, 85–32° W), central Africa (15° S–15° N, 20° W–50° E), SE Asia (10° S–15° N, 90–160° E) and the tropics (15° S–15° N, 180° W–180° E). Here 215 hPa IWC is used as a proxy of deep convection (Jiang et al., 2007, 2011). Over the tropics (Fig. 2a), UT CO anomaly is significantly correlated with CO emission anomaly, and the largest correlation coefficient occurs at 2-month time lag ($r = 0.64$). The correlation with IWC anomaly is relatively weak at zero time lag ($r = 0.31$). However, during some periods (e.g., October 2010–January 2011), there is overlap between peaks of UT CO anomaly and IWC anomaly. This suggests that while surface CO emission controls most of the UT CO anomalies, sometimes convective transport is also important. To evaluate the interannual variation of UT CO in different subregions, we also examined the three tropical continents. Over South America (Fig. 2b), UT CO anomaly is significantly correlated with CO emission anomaly, and the correlation coefficient is largest at 2-month time lag ($r = 0.72$). The IWC anomaly has a weak correlation ($r = 0.25$) with UT CO anomaly at zero time lag. This is similar to the tropics, suggesting that the interannual variation of UT CO over this region mainly follows the changes of surface CO emission, which is consistent with previous studies (e.g., Liu et al., 2010). Over central Africa (Fig. 2c), UT CO anomaly is only significantly correlated with IWC anomaly ($r = 0.39$), not with CO emission. This is not surprising, since the CO transport pattern is different over northern Africa compared to other regions. In boreal winter, the Harmattan winds transport LT CO from the burning region to the Gulf of Guinea where CO is lofted by deep convection and then transported

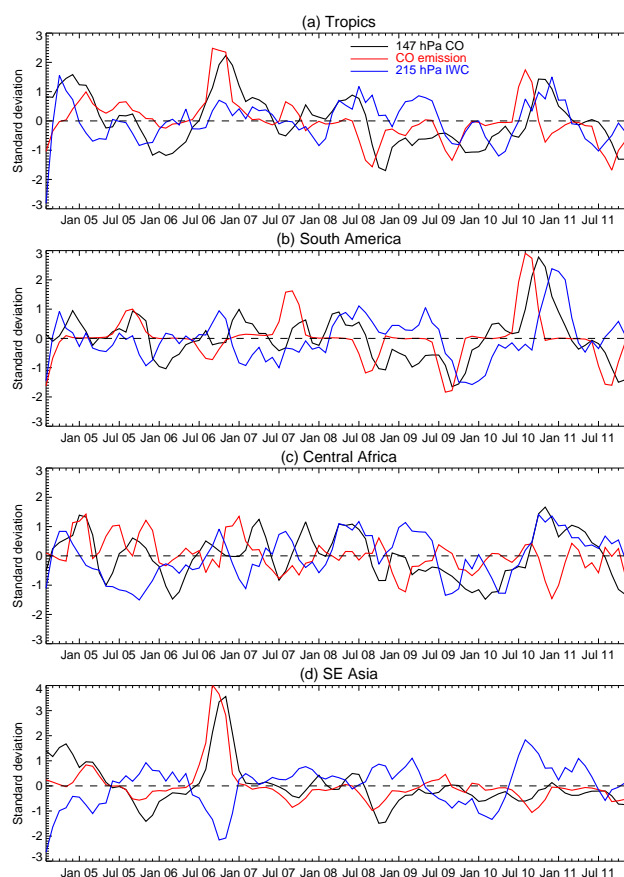


Fig. 2. Time series of monthly anomalies of MLS CO at 147 hPa (black), surface CO emission (red) and MLS ice water content (IWC) at 215 hPa over (a) the tropics (15° S–15° N, 180° W–180° E), (b) South America (15° S–12° N, 85–32° W), (c) central Africa (15° S–15° N, 20° W–50° E), and (d) SE Asia (10° S–15° N, 90–160° E) for the period of August 2004–December 2011.

back across West Africa by horizontal winds in the UT (Liu et al., 2010). Thus, the relationships between UT CO, surface CO emission and convection are complicated over this region due to the involved horizontal transport process. Over SE Asia (Fig. 2d), both CO emission and IWC anomalies are significantly correlated with UT CO anomaly (0.77 and -0.66 , respectively), suggesting that both CO emission and convective transport are important in determining the interannual variation of UT CO over this region. The negative correlation between UT CO and IWC anomalies over this region is expected from the decrease of convection and increase of CO emission related to the intense drought-induced fires (e.g., Liu et al., 2013; Livesey et al., 2013).

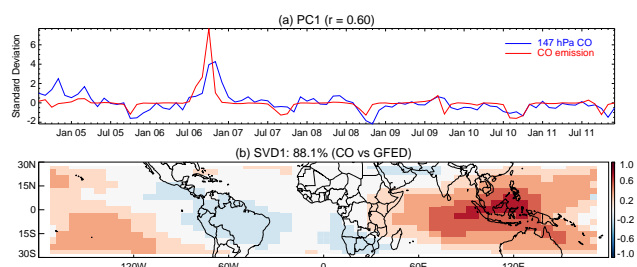


Fig. 3. SVD analysis results of 147 hPa CO and CO emission for the period of August 2004–December 2011: (a) principle components (PCs) of 147 hPa CO (blue) and CO emission (red) for the first SVD mode and (b) heterogeneous correlation map of 147 hPa CO (i.e., correlation between 147 hPa CO and the PC of CO emission) for the first SVD mode.

4 Impacts of CO emission, convection and SST on UT CO interannual variation

We use SVD method to study the coupled relationships between UT CO anomaly and the anomalies of CO emission, convection and SST during the period 08/2004–12/2011. In contrast to the individual EOF analysis performed on the UT CO (Sect. 3), the SVD analysis on two combined fields will identify only those modes of behavior in which the two fields are strongly coupled.

The first SVD mode between 147 hPa CO and CO emission accounts for 88.1 % of the total squared covariance, while the squared covariance explained by the rest modes is much smaller compared to the first mode. Figure 3a shows the two PCs of 147 hPa CO and CO emission for the first SVD mode. The correlation coefficient between the two PCs is 0.6, which is an indicator of the coupling strength. Both PCs have significant correlation with ENSO index (SOI). The coupled spatial patterns of the first SVD mode are shown in Fig. 3b as a heterogeneous correlation map of 147 hPa CO. It shows a center of high correlation over Indonesia and the adjacent Indian Ocean, suggesting the coupling between UT CO and surface CO emission is strongest over this region. Over South America, the correlation is smaller in magnitude than over Indonesia, suggesting the coupled relationship is weaker over this region. The opposite sign between Indonesia and South America indicates the impacts of ENSO. We also examined the second and third SVD modes (not shown here); these modes contribute little (less than 10 %) to the explained squared covariance and have only weak correlations with the climate indices.

Next, we use 215 hPa IWC as a proxy for deep convection and apply SVD analysis to 147 hPa CO and 215 hPa IWC. The first three SVD modes account for 65.0 %, 14.3 % and 7.9 % of the total squared covariance, respectively. The correlation coefficient between the two PCs of the first mode is 0.74 (Fig. 4a). Both PCs have significant correlation with ENSO indices (Niño 3, Niño 4, Niño 3.4 and SOI). The het-

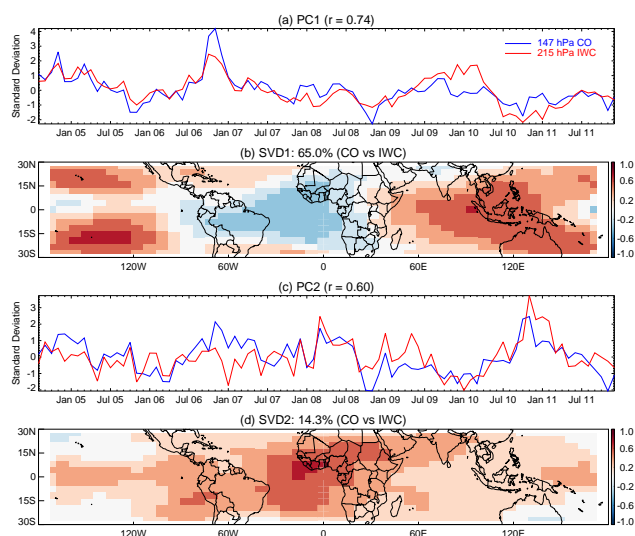


Fig. 4. SVD analysis results of 147 hPa CO and 215 hPa IWC for the period of August 2004–December 2011: (a) principle components (PCs) of 147 hPa CO (blue) and 215 hPa IWC (red) for the first SVD mode, (b) heterogeneous correlation map of 147 hPa CO (i.e., correlation between 147 hPa CO and the PC of 215 hPa IWC) for the first SVD mode, (c) PCs of 147 hPa CO (blue) and 215 hPa IWC (red) for the second SVD mode, and (d) heterogeneous correlation map of 147 hPa CO for the second SVD mode.

erogeneous correlation map of 147 hPa CO (Fig. 4b) shows a zonal dipole between tropical Asia and South America–southern Africa, which suggests the coupling between UT CO and convection is stronger over these regions and mainly affected by ENSO. For the second SVD mode, the correlation coefficient between the two PCs is 0.60 (Fig. 4c). The heterogeneous correlation map of 147 hPa CO (Fig. 4d) shows a high correlation center over the tropical Atlantic Ocean and West Africa, which resembles that of the third REOF mode of 147 hPa CO (Fig. 1g). Thus, this mode may indicate the influence of the Atlantic Ocean. The third SVD mode contributes less than 10 % to the explained squared covariance and is not discussed here.

Finally, we apply SVD analysis to 147 hPa CO and SST to evaluate the coupled relationship between UT CO and transport induced by climate change. The first three SVD modes between 147 hPa CO and SST account for 64.9 %, 16.3 % and 10.1 % of the total squared covariance, respectively. The correlation coefficients between the two PCs of the three leading mode are 0.65, 0.64 and 0.73, respectively (Fig. 5a, c and e). Both PCs of the first SVD mode have significant correlation with ENSO indices (Niño 3, Niño 4, Niño 3.4 and SOI), with largest correlation shown at Niño 4 of 0.53 with UT CO and 0.87 with SST. In fact, each of the three heterogeneous correlation maps of 147 hPa CO (Fig. 5b, d and f), and the correlation between PCs of each mode and various climate indices, are similar to those of the corresponding SVD mode between 147 hPa CO and 215 hPa IWC.

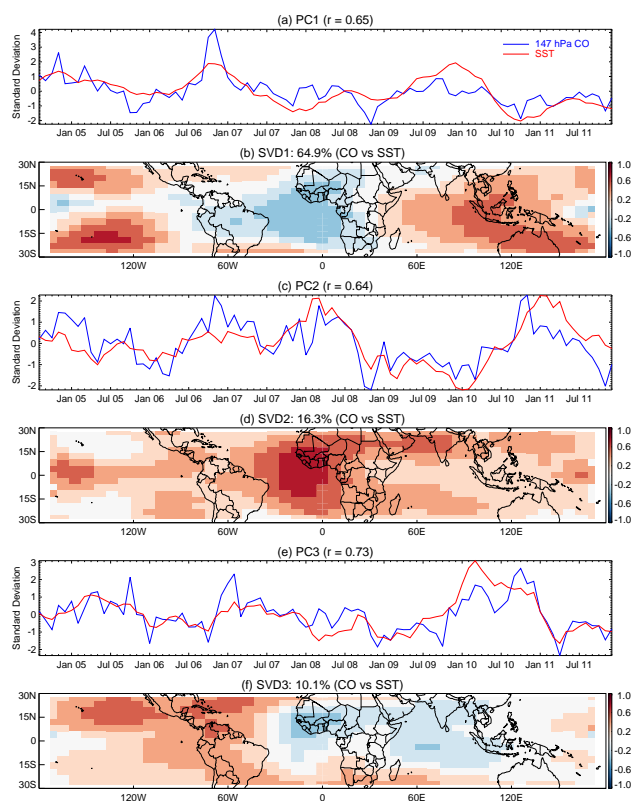


Fig. 5. SVD analysis results of 147 hPa CO and SST for the period of August 2004–December 2011: (a) principle components (PCs) of 147 hPa CO (blue) and SST (red) for the first SVD mode, (b) heterogeneous correlation map of 147 hPa CO (i.e., correlation between 147 hPa CO and the PC of SST) for the first SVD mode, (c) PCs of 147 hPa CO (blue) and SST (red) for the second SVD mode, (d) heterogeneous correlation map of 147 hPa CO for the second SVD mode, (e) PCs of 147 hPa CO (blue) and SST (red) for the third SVD mode, and (f) heterogeneous correlation map of 147 hPa CO for the third SVD mode.

The SVD analyses above suggested that ENSO has significant impacts on the coupled relationship between UT CO and surface CO emission, convection, and SST. The coupling is strongest over the Indonesian region. The similarity between SVD analyses of CO–SST and CO–IWC suggests that SST anomaly plays an important role in deep convection changes, which affect the vertical transport of CO. In the following section, we will investigate the impacts of different ENSO phases on CO transport from the surface to the UT.

5 Impact of ENSO on UT CO interannual variation

Since the launch of Aura, there have been several ENSO periods: 2004, 2006 and 2009 are typical El Niño years, while 2005, 2007 and 2010 are typical La Niña years (Table 1, based on a threshold of $\pm 0.5^\circ\text{C}$ for the Oceanic Niño Index (ONI), <http://www.cpc.ncep.noaa.gov/products/>

Table 1. El Niño and La Niña years since 2004. “CP-El Niño” represents central Pacific El Niño, and “EP-El Niño” represents eastern Pacific El Niño.

El Niño years	La Niña years
2004/2005 (CP-El Niño)	2005/2006
2006/2007 (EP-El Niño)	2007/2008
2009/2010 (CP-El Niño)	2010/2011

analysis_monitoring/ensostuff/ensoyears.shtml). During the 2004/05 and 2009/10 El Niño, the strong positive SST anomalies were mainly located in the central Pacific, while during the 2006/07 El Niño, there were also strong SST anomalies in the eastern Pacific (Yeh et al., 2009; Lee et al., 2010; Su and Jiang, 2013).

Since the strongest biomass burning in South America and central Africa occurs in boreal fall (Huang et al., 2012), here we choose September–November (SON) as the focused period to study the differences of CO transport to the UT between different ENSO phases. The distributions of seasonal average CO and IWC anomalies at 215 hPa are shown in Figure 6. The anomalies are calculated as the seasonal mean of each year minus the 2005–2011 climatological mean. Over Indonesia, UT CO anomaly generally shows opposite sign to that of co-located IWC, which is consistent with the negative correlation between UT CO and IWC anomalies discussed in Sect. 3. In general, UT CO shows positive anomalies over the Indonesian region and Indian Ocean in El Niño years, compared to negative anomalies over the same region in La Niña years. Over South America, UT CO shows consistently strong positive anomalies in La Niña years, while the anomalies are not consistent in El Niño years. For example, there were moderate positive UT CO anomalies in 2004, compared to strong negative anomalies in 2009. Another region that shows distinct ENSO impacts is the central Pacific (around the dateline), where positive (negative) UT CO and IWC anomalies are co-located during El Niño (La Niña) years, suggesting that the two ENSO phases have totally different impacts on the convective transport, which is important in determining UT CO concentration over this region. In contrast to the strong variations of UT CO and IWC anomalies among different El Niño events, the anomaly patterns of UT CO and IWC show much less variation among different La Niña events.

Why are the patterns of the UT CO anomalies so different between different ENSO phases? To explore this question, we carried out the analyses through two ways: one way is to analyze the differences of surface emission and convection, and the other way is to analyze the differences of CO transport pathways. The distributions of GFED CO emission and GPCP precipitation anomalies are shown in Fig. 7. During the 2004 and 2006 El Niño periods, CO emissions show positive anomalies over Indonesia and northern Australia

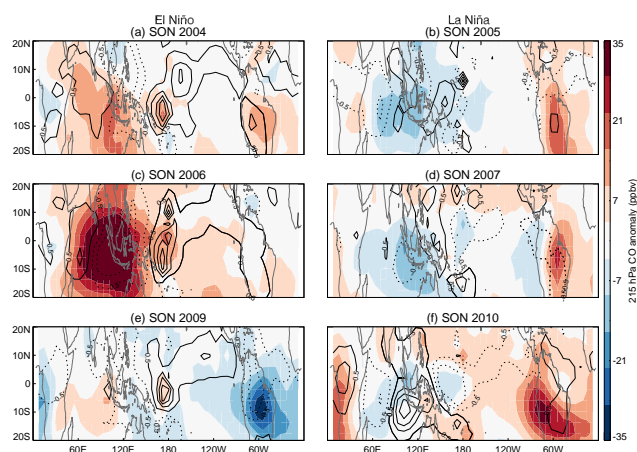


Fig. 6. Seasonal (SON) mean distributions of CO (shaded contour) and IWC (line contour) anomalies in the upper troposphere (215 hPa) during (a) 2004, (b) 2005, (c) 2006, (d) 2007, (e) 2009 and (f) 2010. The IWC contour interval is 1 mg m^{-3} . The solid line represents positive IWC anomaly, and the dotted line represents negative IWC anomaly.

and negative anomalies over South America, which was also found in previous studies (e.g., Logan et al., 2008; Chandra et al., 2009). However, in 2009 El Niño, there was a negative emission anomaly over Indonesia, and a much stronger negative anomaly over South America than the previous two events. This may explain the weak CO anomaly over Indonesia and strong negative CO anomaly over South America at 215 hPa (Fig. 6). In all three El Niño events, positive precipitation anomalies occurred over the central Pacific, consistent with the positive 215 hPa IWC anomalies discussed before. During La Niña periods, CO emissions generally show opposite anomalies over Indonesia, Australia and South America compared to those during El Niño periods.

To investigate the differences of CO transport pathways between different ENSO phases, we performed analysis using the pathway auto-identification method developed in Huang et al. (2012). Since CloudSat was launched in 2006, here we only have two El Niño years (2006 and 2009) and two La Niña years (2007 and 2010) for the analysis. First, we calculate the relative frequency of each transport pathway, which is defined as

$$\text{freq}_i = \frac{N_i}{N_{\text{total}}}, \quad (2)$$

where freq_i is the relative frequency of the i th pathway within a 4° latitude \times 8° longitude grid box, N_i is the number of CO increase cases associated with the i th pathway and N_{total} is the total number of CO increase cases within the same grid box. The results are shown in Figs. 8 and 9, for the “local convection” and the “LT advection \rightarrow convection” pathway, respectively. The “local convection” pathway occurred more frequently over South America than over southern Africa, while the frequency was lowest over the Indone-

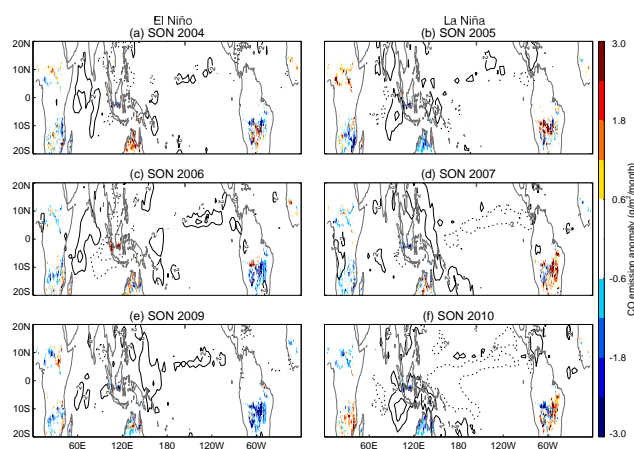


Fig. 7. As in Fig. 6, but for surface CO emission (shaded contour) and precipitation (line contour) anomalies. The precipitation contour interval is 4 mm d^{-1} . The solid line represents positive precipitation anomaly, and the dotted line represents negative precipitation anomaly.

sian region (Fig. 8). During El Niño periods, although the UT CO concentration over South America was much higher in 2006 than in 2009 (Fig. 6), the frequency of “local convection” pathway did not show much difference. During La Niña periods, the “local convection” pathway occurred more frequently in 2007 than in 2010 over South America, but the UT CO was higher in 2010. Thus, the interannual variation of the frequency of “local convection” pathway appeared to be not consistent with the interannual variation of UT CO over South America, and this conclusion also applied to other tropical continents. Besides, the frequency of “local convection” pathway did not show a clear difference between different ENSO phases. For the “LT advection \rightarrow convection” pathway, it occurred more frequently over maritime areas than over continents, especially over the tropical western Pacific and northern Indian Ocean (Fig. 9). The frequency of “LT advection \rightarrow convection” pathway appeared to be higher over the west-central Pacific (near Indonesia) during El Niño years than during La Niña years, which may account for the UT CO differences over this region between different ENSO phases (Fig. 6).

Second, we calculate the average increase of CO concentration at 215 hPa associated with the “local convection” ($\Delta\text{CO}_{\text{local}}$) and the “LT advection \rightarrow convection” ($\Delta\text{CO}_{\text{LT-adv}}$) pathway, and the results are shown in Figs. 10 and 11, respectively. In general, the interannual variation of $\Delta\text{CO}_{\text{local}}$ is consistent with the interannual variation of UT CO over the tropical continents. For example, the higher CO concentrations over South America during 2006 than 2009 (both are El Niño years), or during 2010 than 2007 (both are La Niña years), corresponded to the higher $\Delta\text{CO}_{\text{local}}$ during that year. Besides, $\Delta\text{CO}_{\text{local}}$ appeared to be higher over Indonesia–Australia and lower over South America during El

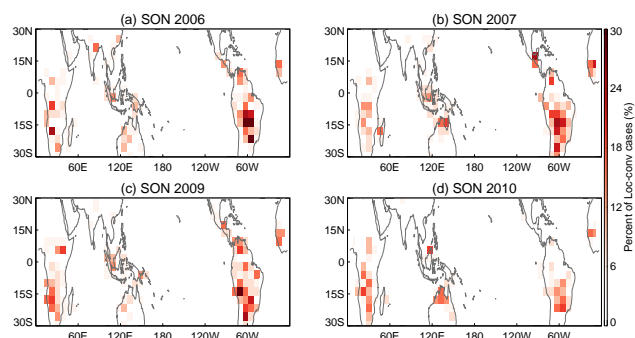


Fig. 8. Spatial distributions of the relative frequency (percentage) of the “local convection” transport pathway within each 4° latitude \times 8° longitude grid box during (a) SON 2006, (b) SON 2007, (c) SON 2009 and (d) SON 2010.

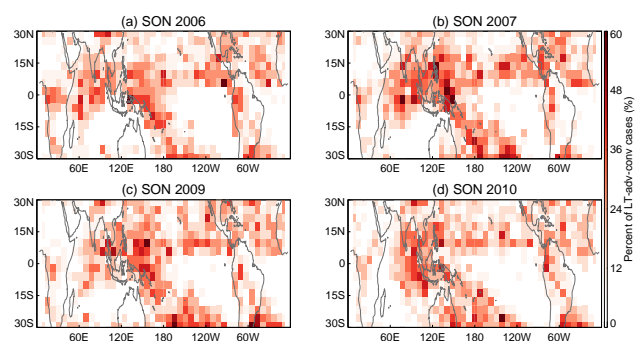


Fig. 9. As in Fig. 8, but for the “LT advection \rightarrow convection” transport pathway.

Niño years than during La Niña years, which indicates clear differences of CO transport between different ENSO phases. Compared to other years, $\Delta\text{CO}_{\text{LT-adv}}$ was higher over the Indonesian region in 2006 and over southern South America ($15\text{--}30^\circ$ S) in 2010 (Fig. 11). Thus, the interannual variation of $\Delta\text{CO}_{\text{LT-adv}}$ cannot explain the interannual variation of CO in the tropical UT. In addition, $\Delta\text{CO}_{\text{LT-adv}}$ did not show clear difference between different ENSO phases over the tropics.

To further quantify the differences of CO transport from the surface to the UT between two different El Niño events (2006 and 2009), we choose three tropical land regions – South America (24° S– 12° N, $88\text{--}32^\circ$ W), central Africa (20° S– 20° N, 16° W– 40° E) and Indonesia (10° S– 10° N, $90\text{--}160^\circ$ E) – since they represent the main CO source regions and/or UT CO centers. The results are shown in Table 2. Over central Africa, although the number of “local convection” events was smaller in 2006 than in 2009, the number of “LT advection \rightarrow convection” events was larger. Thus the total number of transport events was nearly equal between the 2 years. In addition, the average CO increase associated with either pathway was also comparable between 2006 and 2009. Thus, the overall CO transport over this region did not show much difference between the 2 years. Over

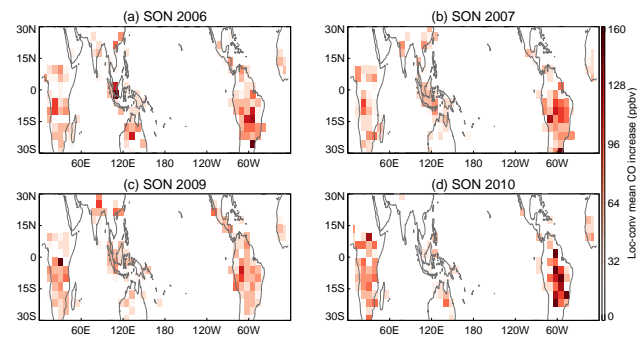


Fig. 10. Spatial distributions of the average increase of CO associated with the “local convection” transport pathway within each 4° latitude \times 8° longitude grid box during (a) SON 2006, (b) SON 2007, (c) SON 2009 and (d) SON 2010.

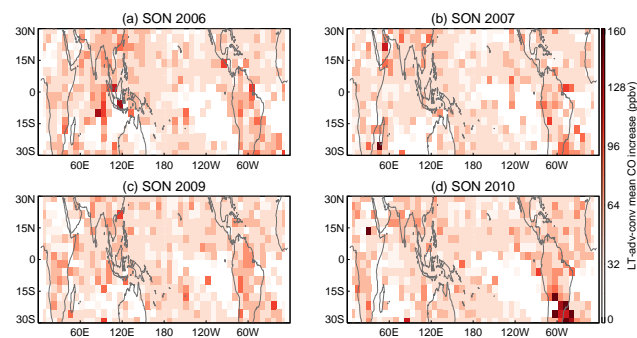


Fig. 11. As in Fig. 10, but for the “LT advection \rightarrow convection” transport pathway.

South America, the number of “LT advection \rightarrow convection” events was much larger in 2006 than in 2009, while the number of “local convection” events was nearly equal. However, $\Delta\text{CO}_{\text{local}}$ was significantly lower in 2009 (58.6 ppbv) than in 2006 (75.5 ppbv), while $\Delta\text{CO}_{\text{LT-adv}}$ was nearly equal. This may be the reason for the strong negative UT CO anomaly in 2009 over this region. Over Indonesia, the numbers of both pathway events were larger in 2009 than in 2006. However, a much stronger positive anomaly of UT CO occurred in 2006 (Fig. 6). To explain this, we need to check ΔCO associated with each pathway. Indeed, $\Delta\text{CO}_{\text{local}}$ was significantly higher in 2006 (73.8 ppbv) than in 2009 (47.8 ppbv). Although $\Delta\text{CO}_{\text{LT-adv}}$ was also higher in 2006, the difference between the 2 years was much less than that of $\Delta\text{CO}_{\text{local}}$. The reason why fewer transport events were identified in 2006 than 2009 over Indonesia may be due to higher background CO concentrations in the UT, which are used to determine CO changes for identifying transport pathways.

6 Conclusions

In this study, we have identified the dominant modes of the interannual variation of tropical UT CO by using rotated EOF

Table 2. Results of CO transport pathway analyses over central Africa (AF), South America (SA) and Indonesia (IN). From left to right, the first column indicates the regions, the second and seventh columns the number of “local convection” events, the third and eighth columns the average CO increase (ppbv) associated with “local convection” pathway, the fourth and ninth columns the number of “LT advection → convection” events, the fifth and tenth columns the average CO increase (ppbv) associated with “LT advection → convection” pathway, and the sixth and eleventh columns the total number of CO transport events during SON in each year.

	2006 SON					2009 SON				
	loc-conv		LT adv-conv		total	loc-conv		LT adv-conv		total
	no. of events	ΔCO	no. of events	ΔCO	no. of events	no. of events	ΔCO	no. of events	ΔCO	no. of events
AF	81	59.88	240	43.52	321	104	53.61	199	47.5	303
SA	154	75.46	358	51.59	512	157	58.6	319	53.23	476
IN	32	73.78	281	53.23	313	43	47.78	344	46.07	387

analysis, and evaluated the coupled relationships between UT CO and its governing factors (e.g., CO emission and convection) by using SVD analysis. The differences of CO emission, convection and transport pathways between different ENSO phases are investigated by using satellite observation data and pathway auto-identification method developed in our previous study. The main conclusions are summarized as follows: Indonesia is the most significant tropical land region that affects UT CO interannual variation, as suggested by the first REOF mode of UT CO. South America and central Africa have a secondary yet significant contribution to the interannual variation of tropical UT CO. Among the various climate conditions, ENSO has significant impacts on the time evolution of the first REOF mode.

Over South America, the interannual variation of UT CO is mainly affected by the interannual variation of CO emission, as suggested by the significant correlation between the monthly anomalies of UT CO and CO emission. Over central Africa, UT CO is not closely correlated with emission or convection, partly due to the involved horizontal transport process. Over SE Asia, both CO emission and convective transport are important in determining the interannual variation of UT CO. Over the whole tropics, the interannual variation of UT CO is mainly affected by the interannual variation of CO emission, which is similar to that over South America. The SVD analyses suggest that ENSO has important effects on the coupled relationships between UT CO and CO emission, UT CO and convection, as well as UT CO and SST. These couplings are strongest over the Indonesian region.

The impacts of different ENSO phases on the interannual variation of CO in the tropical UT are analyzed through two ways: factor analysis and transport pathway analysis. During boreal fall season, UT CO shows positive anomalies over the Indonesian region and Indian Ocean in El Niño years, compared to negative anomalies over the same region in La Niña years. This is closely related to the in-phase CO emission anomalies. UT CO shows consistently strong positive anomalies over South America in La Niña years, which is associated with positive CO emission anomalies. Over the central Pacific (around the dateline), positive (negative) UT

CO anomalies occur in El Niño (La Niña) years, mainly due to positive (negative) convection anomalies. The anomalies of UT CO and convection show much stronger variations among different El Niño events than among different La Niña events.

Through the transport pathway analysis, we found that the interannual variation of UT CO over the tropical continents is consistent with that of the average CO increase associated with the “local convection” pathway, instead of the relative frequency of this pathway. The relative frequency of the “LT advection → convection” pathway appears to be the factor that accounts for the UT CO differences over the west-central Pacific between different ENSO phases. Besides, different ENSO phases have different impacts on the average CO transported by the “local convection” pathway, which appears to be higher over Indonesia–Australia and lower over South America during El Niño years than during La Niña years. Although both 2006 and 2009 are El Niño years, the SST patterns are totally different. The results of transport pathway analysis suggest that the average CO transported per event of “local convection”, instead of the number of transport events, is the factor that accounts for the UT CO difference between these two El Niño periods over South America and Indonesia. The contribution from the “LT advection → convection” pathway is much smaller and negligible compared to the “local convection” pathway.

Although previous studies have found that ENSO has significant impact on the interannual variation of UT CO (e.g., Edwards et al., 2006b; Duncan and Logan, 2008), this work is consistent with previous findings by directly evaluating the UT CO anomaly field. Besides, we found that different ENSO phases have rather different impacts on spatial pattern of the UT CO, which is related to the differences in CO transport. Although we have analyzed the impacts of different ENSO phases and events on the interannual variation of tropical UT CO, due to the limited satellite observations, we only have a relatively short period of data for the transport pathway analysis; whether these characteristics and differences apply to other El Niño/La Niña events still needs further studies.

Acknowledgements. This research is supported by the NASA Aura Science Team (AST) program (NNX09AD85G), the Jackson School of Geosciences at the University of Texas at Austin, and the Jet Propulsion Laboratory, California Institute of Technology, under contract with NASA. We acknowledge the NASA CloudSat project for the CloudSat data. We also appreciate the comments from three reviewers and editor B. N. Duncan that led to significant improvements of the manuscript.

Edited by: B. N. Duncan

References

- Adler, R. F., Huffman, G. J., Chang, A., Ferraro, R., Xie, P. P., Janowiak, J., Rudolf, B., Schneider, U., Curtis, S., and Bolvin, D.: The version-2 global precipitation climatology project (GPCP) monthly precipitation analysis (1979-present), *J. Hydrometeorol.*, 4, 1147–1167, 2003.
- Andreae, M. O., Artaxo, P., Fischer, H., Freitas, S. R., Gregoire, J. M., Hansel, A., Hoor, P., Kormann, R., Krejci, R., Lange, L., Lelieveld, J., Lindinger, W., Longo, K., Peters, W., de Reus, M., Scheeren, B., Dias, M. A. F. S., Strom, J., van Velthoven, P. F. J., and Williams, J.: Transport of biomass burning smoke to the upper troposphere by deep convection in the equatorial region, *Geophys. Res. Lett.*, 28, 951–954, 2001.
- Andreae, M. O., Rosenfeld, D., Artaxo, P., Costa, A. A., Frank, G. P., Longo, K. M., and Silva-Dias, M. A. F.: Smoking rain clouds over the Amazon, *Science*, 303, 1337–1342, 2004.
- Ashok, K., Behera, S. K., Rao, S. A., Weng, H., and Yamagata, T.: El Niño Modoki and its possible teleconnection, *J. Geophys. Res.*, 112, C11007, doi:10.1029/2006jc003798, 2007.
- Bretherton, C. S., Widmann, M., Dymnikov, V. P., Wallace, J. M., and Bladé, I.: The Effective Number of Spatial Degrees of Freedom of a Time-Varying Field, *J. Climate*, 12, 1990–2009, 1999.
- Chandra, S., Ziemke, J. R., Duncan, B. N., Diehl, T. L., Livesey, N. J., and Froidevaux, L.: Effects of the 2006 El Niño on tropospheric ozone and carbon monoxide: implications for dynamics and biomass burning, *Atmos. Chem. Phys.*, 9, 4239–4249, doi:10.5194/acp-9-4239-2009, 2009.
- CloudSat project: CloudSat Standard Data Products Handbook, Cooperative Institutes for Research in the Atmosphere, Colorado State University, Fort Collins, CO, 2008.
- Daniel, J. S. and Solomon, S.: On the climate forcing of carbon monoxide, *J. Geophys. Res.*, 103, 13249–13260, 1998.
- Duncan, B. N. and Logan, J. A.: Model analysis of the factors regulating the trends and variability of carbon monoxide between 1988 and 1997, *Atmos. Chem. Phys.*, 8, 7389–7403, doi:10.5194/acp-8-7389-2008, 2008.
- Duncan, B. N., Strahan, S. E., Yoshida, Y., Steenrod, S. D., and Livesey, N.: Model study of the cross-tropopause transport of biomass burning pollution, *Atmos. Chem. Phys.*, 7, 3713–3736, doi:10.5194/acp-7-3713-2007, 2007.
- Edwards, D. P., Emmons, L. K., Gille, J. C., Chu, A., Attie, J. L., Giglio, L., Wood, S. W., Haywood, J., Deeter, M. N., Massie, S. T., Ziskin, D. C., and Drummond, J. R.: Satellite-observed pollution from Southern Hemisphere biomass burning, *J. Geophys. Res.-Atmos.*, 111, D14312, doi:10.1029/2005jd006655, 2006a.
- Edwards, D. P., Petron, G., Novelli, P. C., Emmons, L. K., Gille, J. C., and Drummond, J. R.: Southern Hemisphere carbon monoxide interannual variability observed by Terra/Measurement of Pollution in the Troposphere (MOPITT), *J. Geophys. Res.-Atmos.*, 111, D16303, doi:10.1029/2006jd007079, 2006b.
- Folkens, I., Chatfield, R., Baumgardner, D., and Proffitt, M.: Biomass burning and deep convection in southeastern Asia: Results from ASHOC/MAESA, *J. Geophys. Res.-Atmos.*, 102, 13291–13299, 1997.
- Giglio, L., van der Werf, G. R., Randerson, J. T., Collatz, G. J., and Kasibhatla, P.: Global estimation of burned area using MODIS active fire observations, *Atmos. Chem. Phys.*, 6, 957–974, doi:10.5194/acp-6-957-2006, 2006.
- Giglio, L., Randerson, J. T., van der Werf, G. R., Kasibhatla, P. S., Collatz, G. J., Morton, D. C., and DeFries, R. S.: Assessing variability and long-term trends in burned area by merging multiple satellite fire products, *Biogeosciences*, 7, 1171–1186, doi:10.5194/bg-7-1171-2010, 2010.
- Gonzi, S. and Palmer, P. I.: Vertical transport of surface fire emissions observed from space, *J. Geophys. Res.*, 115, D02306, doi:10.1029/2009JD012053, 2010.
- Huang, L., Fu, R., Jiang, J. H., Wright, J. S., and Luo, M.: Geographic and seasonal distributions of CO transport pathways and their roles in determining CO centers in the upper troposphere, *Atmos. Chem. Phys.*, 12, 4683–4698, doi:10.5194/acp-12-4683-2012, 2012.
- Jiang, J. H., Livesey, N. J., Su, H., Neary, L., McConnell, J. C., and Richards, N. A. D.: Connecting surface emissions, convective uplifting, and long-range transport of carbon monoxide in the upper troposphere: New observations from the Aura Microwave Limb Sounder, *Geophys. Res. Lett.*, 34, L18812, doi:10.1029/2007gl030638, 2007.
- Jiang, J. H., Su, H., Zhai, C., Massie, S. T., Schoeberl, M. R., Colarco, P. R., Platnick, S., Gu, Y., and Liou, K.-N.: Influence of convection and aerosol pollution on ice cloud particle effective radius, *Atmos. Chem. Phys.*, 11, 457–463, doi:10.5194/acp-11-457-2011, 2011.
- Kaiser, H. F.: The varimax criterion for analytic rotation in factor analysis, *Psychometrika*, 23, 187–200, 1958.
- Kao, H. Y. and Yu, J. Y.: Contrasting eastern-Pacific and central-Pacific types of ENSO, *J. Climate*, 22, 615–632, 2009.
- Kug, J. S., Jin, F. F., and An, S. I.: Two Types of El Niño Events: Cold Tongue El Niño and Warm Pool El Niño, *J. Climate*, 22, 1499–1515, doi:10.1175/2008jcli2624.1, 2009.
- Lee, T., Hobbs, W. R., Willis, J. K., Halkides, D., Fukumori, I., Armstrong, E. M., Hayashi, A. K., Liu, W. T., Patzert, W., and Wang, O.: Record warming in the South Pacific and western Antarctica associated with the strong central-Pacific El Niño in 2009–10, *Geophys. Res. Lett.*, 37, L19704, doi:10.1029/2010gl044865, 2010.
- Liu, C. T., Zipser, E., Garrett, T., Jiang, J. H., and Su, H.: How do the water vapor and carbon monoxide “tape recorders” start near the tropical tropopause?, *Geophys. Res. Lett.*, 34, L09804, doi:10.1029/2006gl029234, 2007.
- Liu, Junhua, Logan, J. A., Jones, D. B. A., Livesey, N. J., Megretskaja, I., Carouge, C., and Nedelec, P.: Analysis of CO in the tropical troposphere using Aura satellite data and the GEOS-Chem model: insights into transport characteristics of the GEOS meteorological products, *Atmos. Chem. Phys.*, 10, 12207–12232, doi:10.5194/acp-10-12207-2010, 2010.

- Liu, J., Logan, J. A., Murray, L. T., Pumphrey, H. C., Schwartz, M. J., and Megretskaia, I. A.: Transport analysis and source attribution of seasonal and interannual variability of CO in the tropical upper troposphere and lower stratosphere, *Atmos. Chem. Phys.*, 13, 129–146, doi:10.5194/acp-13-129-2013, 2013.
- Livesey, N. J., Filipiak, M. J., Froidevaux, L., Read, W. G., Lambert, A., Santee, M. L., Jiang, J. H., Pumphrey, H. C., Waters, J. W., Cofield, R. E., Cuddy, D. T., Daffer, W. H., Drouin, B. J., Fuller, R. A., Jarnot, R. F., Jiang, Y. B., Knosp, B. W., Li, Q. B., Perun, V. S., Schwartz, M. J., Snyder, W. V., Stek, P. C., Thurstans, R. P., Wagner, P. A., Avery, M., Browell, E. V., Cammas, J. P., Christensen, L. E., Diskin, G. S., Gao, R. S., Jost, H. J., Loewenstein, M., Lopez, J. D., Nedelec, P., Osterman, G. B., Sachse, G. W., and Webster, C. R.: Validation of Aura Microwave Limb Sounder O-3 and CO observations in the upper troposphere and lower stratosphere, *J. Geophys. Res.-Atmos.*, 113, D15S02, doi:10.1029/2007jd008805, 2008.
- Livesey, N. J., Read, W. G., Froidevaux, L., Lambert, A., and Manney, G. L.: EOS MLS version 3.3 Level 2 data quality and description document, Jet Propulsion Laboratory, California Institute of Technology, Pasadena, CA, 2011.
- Livesey, N. J., Logan, J. A., Santee, M. L., Waters, J. W., Doherty, R. M., Read, W. G., Froidevaux, L., and Jiang, J. H.: Interrelated variations of O₃, CO and deep convection in the tropical/subtropical upper troposphere observed by the Aura Microwave Limb Sounder (MLS) during 2004–2011, *Atmos. Chem. Phys.*, 13, 579–598, doi:10.5194/acp-13-579-2013, 2013.
- Livezey, R. E. and Chen, W. Y.: Statistical Field Significance and its Determination by Monte Carlo Techniques, *Mon. Weather Rev.*, 111, 46–59, 1983.
- Logan, J. A., Megretskaia, I., Nassar, R., Murray, L. T., Zhang, L., Bowman, K. W., Worden, H. M., and Luo, M.: Effects of the 2006 El Niño on tropospheric composition as revealed by data from the Tropospheric Emission Spectrometer (TES), *Geophys. Res. Lett.*, 35, L03816, doi:10.1029/2007GL031698, 2008.
- Lorenz, E. N.: Empirical orthogonal functions and statistical weather prediction, Technical report, Statistical Forecast Project Report 1, Dept. of Meteor., MIT, 49 pp., 1956.
- Mu, M., Randerson, J. T., van der Werf, G. R., Giglio, L., Kasibhatla, P., Morton, D., Collatz, G. J., DeFries, R. S., Hyer, E. J., Prins, E. M., Griffith, D. W. T., Wunch, D., Toon, G. C., Sherlock, V., and Wennberg, P. O.: Daily and 3-hourly variability in global fire emissions and consequences for atmospheric model predictions of carbon monoxide, *J. Geophys. Res.-Atmos.*, 116, D24303, doi:10.1029/2011jd016245, 2011.
- North, G. R., Bell, T. L., Cahalan, R. F., and Moeng, F. J.: Sampling errors in the estimation of empirical orthogonal functions, *Mon. Weather Rev.*, 110, 699–706, 1982.
- Novelli, P., Masarie, K., and Lang, P.: Distributions and recent changes of carbon monoxide in the lower troposphere, *J. Geophys. Res.*, 103, 19015–19033, 1998.
- Pickering, K. E., Thompson, A. M., Wang, Y. S., Tao, W. K., McNamara, D. P., Kirchhoff, V. W. J. H., Heikes, B. G., Sachse, G. W., Bradshaw, J. D., Gregory, G. L., and Blake, D. R.: Convective transport of biomass burning emissions over Brazil during TRACE A, *J. Geophys. Res.-Atmos.*, 101, 23993–24012, 1996.
- Reynolds, R. W., Rayner, N. A., Smith, T. M., Stokes, D. C., and Wang, W.: An improved in situ and satellite SST analysis for climate, *J. Climate*, 15, 1609–1625, 2002.
- Ricaud, P., Barret, B., Attié, J.-L., Motte, E., Le Flochmoën, E., Teysse, H., Peuch, V.-H., Livesey, N., Lambert, A., and Pommereau, J.-P.: Impact of land convection on troposphere-stratosphere exchange in the tropics, *Atmos. Chem. Phys.*, 7, 5639–5657, doi:10.5194/acp-7-5639-2007, 2007.
- Richman, M. B.: Rotation of principal components, *J. Climatol.*, 6, 293–335. doi:10.1002/joc.3370060305, 1986.
- Schoeberl, M. R., Duncan, B. N., Douglass, A. R., Waters, J., Livesey, N., Read, W., and Filipiak, M.: The carbon monoxide tape recorder, *Geophys. Res. Lett.*, 33, L12811, doi:10.1029/2006gl026178, 2006.
- Stephens, G. L., Vane, D. G., Boain, R. J., Mace, G. G., Sassen, K., Wang, Z. E., Illingworth, A. J., O'Connor, E. J., Rossow, W. B., Durden, S. L., Miller, S. D., Austin, R. T., Benedetti, A., Mitrescu, C., and Team, C. S.: The cloudsat mission and the a-train – A new dimension of space-based observations of clouds and precipitation, *B. Am. Meteorol. Soc.*, 83, 1771–1790, doi:10.1175/Bams-83-12-1771, 2002.
- Su, H. and Jiang, J. H.: Tropical clouds and circulation changes during the 2006/07 and 2009/10 El Niños, *J. Climate*, 26, 399–413, doi:10.1175/JCLI-D-12-00152.1, 2013.
- Thompson, A. M.: The oxidizing capacity of the earth's atmosphere: probable past and future changes, *Science*, 256, 1157–1165, doi:10.1126/science.256.5060.1157, 1992.
- Thompson, A. M., Pickering, K. E., McNamara, D. P., Schoeberl, M. R., Hudson, R. D., Kim, J. H., Browell, E. V., Kirchhoff, V. W. J. H., and Nganga, D.: Where did tropospheric ozone over southern Africa and the tropical Atlantic come from in October 1992? Insights from TOMS, GTE TRACE A, and SAFARI 1992, *J. Geophys. Res.-Atmos.*, 101, 24251–24278, 1996.
- van der Werf, G. R., Randerson, J. T., Giglio, L., Collatz, G. J., Mu, M., Kasibhatla, P. S., Morton, D. C., DeFries, R. S., Jin, Y., and van Leeuwen, T. T.: Global fire emissions and the contribution of deforestation, savanna, forest, agricultural, and peat fires (1997–2009), *Atmos. Chem. Phys.*, 10, 11707–11735, doi:10.5194/acp-10-11707-2010, 2010.
- Wallace, J., Smith, C., and Bretherton, C.: Singular value decomposition of wintertime sea surface temperature and 500-mb height anomalies, *J. Climate*, 5, 561–576, 1992.
- Waters, J. W., Froidevaux, L., Harwood, R. S., Jarnot, R. F., Pickett, H. M., Read, W. G., Siegel, P. H., Cofield, R. E., Filipiak, M. J., Flower, D. A., Holden, J. R., Lau, G. K., Livesey, N. J., Manney, G. L., Pumphrey, H. C., Santee, M. L., Wu, D. L., Cuddy, D. T., Lay, R. R., Loo, M. S., Perun, V. S., Schwartz, M. J., Stek, P. C., Thurstans, R. P., Chandra, K. M., Chavez, M. C., Chen, G., Boyles, M. A., Chudasama, B. V., Dodge, R., Fuller, R. A., Girard, M. A., Jiang, J. H., Jiang, Y., Knosp, B. W., LaBelle, R. C., Lam, J. C., Lee, K. A., Miller, D., Oswald, J. E., Patel, N. C., Pukala, D. M., Quintero, O., Scaff, D. M., Snyder, W. V., Tope, M. C., Wagner, P. A., and Walch, M. J.: The Earth Observing System Microwave Limb Sounder (EOS MLS) on the Aura satellite, *IEEE Trans. Geosci. Remote Sens.*, 44, 1075–1092, 2006.
- Wotawa, G., Novelli, P., Trainer, M., and Granier, C.: Inter-Annual Variability of Summertime CO Concentrations in the Northern Hemisphere Explained by Boreal Forest Fires in North America and Russia, *Geophys. Res. Lett.*, 28, 4575–4578, 2001.
- Wu, D. L., Jiang, J. H., Read, W. G., Austin, R. T., David, C. P., Lambert, A., Stephens, G. L., Vane, D. G., and Waters, J. W.: Validation of Aura MLS cloud Ice Water Con-

tent (IWC) measurements, *J. Geophys. Res.*, 113, D15S10, doi:10.1029/2007JD008931, 2008.

Yeh, S. W., Kug, J. S., Dewitte, B., Kwon, M. H., Kirtman, B. P., and Jin, F. F.: El Niño in a changing climate, *Nature*, 461, 511–514, doi:10.1038/Nature08316, 2009.